Electrical and magnetic properties of silicon carbide composites with titanium and niobium carbide as sintering aids

R. Bystrický[1, 6, *], M. Škrátek[2], J. Rusnák[1, 3], M. Precner[4], M. Ťapajna[4], M. Hnatko[1, 5], P. Šajgalík[1, 5]

[1]Institute of Inorganic Chemistry, Slovak Academy of Sciences, Dúbravská cesta 9, 841 04 Bratislava

[2]Institute of Measurement Science, Slovak Academy of Sciences, Dúbravská cesta 9, 841 04 Bratislava

[3]Institute of Physics, Slovak Academy of Sciences, Dúbravská cesta 9, 841 04, Bratislava

[4]Institute of Electrical Engineering, Slovak Academy of Sciences, Dúbravská cesta 9, 841 04 Bratislava

[5]Centre for Advanced Materials Application (CEMEA), Slovak Academy of Science (SAS), Dúbravská cesta 9, 841 04, Bratislava, Slovakia

[6]Laboratory for Advanced materials, Faculty of Natural Sciences, Comenius University, 842 15 Bratislava, Slovakia

Abstract

Silicon carbide based composites with 30, 40 and 50 wt. % of of Ti and NbC as sintering additives were prepared by hot-press method. Molar ratio of Ti:NbC was kept at 1:1.8.

* *Corresponding author*. Tel. Tel.: +421-2-59410-427; fax: +421-2-59410-444
email: roman.bystricky@savba.sk (Roman Bystrický)

The two step sintering was performed in order to avoid the squeezing out the melted titanium above 1668 °C. Composite powders were sintered at 1650 °C for 3 h and subsequently at 1850 °C for 1 h under mechanical pressure of 30 MPa in Ar atmosphere. XRD pattern confirmed the formation of (Ti, Nb)C_{ss} in the SiC matrix. Composite with 50 % of Ti-NbC phase showed the extraordinary electrical conductivity of 2.4 x 10^5 S/m which was achieved by homogeneous distribution of Ti and NbC in SiC matrix and forming a continuous conductive network. Prepared composites show complex magnetic properties, diamagnetism originated from SiC matrix, paramagnetism caused by Ti and NbC admixing, as well as weak ferromagnetism probably coming from impurities contained in the initial powders. Samples with 30 and 40 wt. % of Ti and NbC exhibit superconducting state below 2 K.

Keywords: silicon carbide (D), niobium carbide (D), electrical conductivity (c), hot pressing (A)

1. Introduction

Increasing the electrical conductivity of structural ceramics is important for applications that require manufacturing components with complex shapes using the electro-discharge machining (EDM) technique [1-3].

The electrical conductivity of ceramics can be influenced mainly by the composition of grain boundary phase [4-8] as well as by processing conditions [9]. Kim et al. [10] achieved the electrical conductivity of SiC (3 x 10^4 S/m) by nitrogen doping resulting from $Y(NO_3)_3$ as a sintering additive.

A promising approach of influencing the electrical conductivity is a combination of insulating engineering ceramics with electrically conductive phases. Incorporation of

carbon nanostructure (carbon fiber, carbon nanotubes, graphene) into the ceramic matrix led to the improvement of the electrical conductivity of ceramics [11-17]. These nanostructures can form the conductive network within the matrix and can significantly increase the electrical conductivity. On the other hand, there are difficulties with homogeneous distribution of these carbon nanostructures in the matrix and for composites with higher amount of carbon nanostructures is difficult to reach fully dense materials. Both issues result in the degradation of mechanical properties of the prepared composites.

Another good candidate for increasing of the electrical conductivity of ceramics is niobium carbide which has high electrical conductivity (13.5 x 10^3 S/m) as pure phase [18]. In addition, it possesses high stability, high hardness and high wear resistance. Moreover, in combination with Ti helps to densify the SiC ceramics and can significantly increase the electrical conductivity of resulted material [19]. Ti forms TiC at high temperatures, which is another phase with high stability, high hardness and high wear resistance.

Several papers were published during last years, where Ti and NbC were added into SiC matrix to increase the electrical conductivity of resulting composite [19, 20].

Balog et al. prepared such composites and they studied the influence of addition of Ti and NbC into the SiC matrix on the mechanical and electrical properties. The amount of Ti and NbC addition varied from 10 to 90 wt. %. AlN and rare earth oxides were used as sintering additives. Their amount was kept at 13 wt. %. Two step sintering was used in order to densify composite materials, at first the samples were heated up to 1650 °C for 3h and subsequently at 1850 °C for 1h. The hardness and fracture toughness were not substantially changed by the addition of the Ti and NbC phases up to 50 wt. %. An almost linear increase of electrical conductivity up to 80 wt. % of the electrically conductive phase was observed where 4 x 10^4 S/m was achieved [20].

Frajkorova et al. prepared SiC-Ti-NbC composites where no oxide additives were used as sintering additives. Composites with 30, 40, and 50 wt. % of Ti and NbC phase, were sintered at 1850 °C for 1h. Only sample with 50 wt. % of addition of Ti and NbC was fully dense and electrical conductivity reached 3.06 x 10^4 S/m [19].

Present paper has an ambition to present the results of the preparation of the SiC based ceramics with increased electrical conductivity at room temperature and superconductivity at the temperature characteristic for NbC and Ti metals. The appropriate addition of NbC and Ti to the SiC ceramics for reaching these goals will be discussed. Functional properties of ceramics were measured by different methods of physics.

2. Experimental section

2.1. Preparation of composites

The commercially available powders of *β*-SiC (HSC-059, Superior Graphite, USA, mean diameter of 0.55 μm), Ti (TOHO Titanium Co., Japan, mean diameter of 5-10 μm) and NbC (Japan New Metals Co., Japan, mean diameter of 1 μm) were used for the starting mixtures preparation. Impurities in the initial powders (Tab. 1) were determined by X-ray fluorescence spectrometry (ARL Advant´X Intellipower 3600 Wavelength Dispersive X-ray Fluorescence WDXRF).

The SiC-based composites were prepared by the addition of the various amount of electrically conductive Ti-NbC phase (mixture of Ti and NbC in a molar ratio 1:1.8). The chemical composition of starting mixtures is briefly listed in Table 2.

Appropriate amounts of SiC, Ti and NbC were homogenized in distilled water with WC balls by planetary ball mill (Retsch PM 100) at 150 rpm for 1 h. Then such prepared

suspensions were sprayed immediately into the liquid nitrogen in order to prevent separation of phases with different densities (Tab. 3) and subsequently frozen powders were freeze dried.

The pre-pressed pellets were hot pressed in two steps: at 1650 °C for 3 h and at 1850 °C for 1 h under mechanical pressure of 30 MPa in Ar atmosphere. Reference sample without any additives was prepared by hot-press at 1850 °C. Details of sintering process are described in Ref. 21.

2.2. Microstructural characterization

The densities of the samples were measured by Archimedes method in mercury. The theoretical densities were calculated according to the rule of mixtures.

The microstructures were observed by scanning electron microscopy EVO 40HV (Karl Zeiss, Germany). For this purpose, the sintered samples were cut, polished and etched on Femto plasma system (Diener Electronic, Germany, O2:CF4 = 3:7).

Direct microstructural investigations were performed on a probe-corrected Titan Themis 300 (FEI/Thermofisher Scientific, USA) transmission electron microscope in scanning mode (STEM) at 200 kV accelerating voltage equipped with the EDS system (Super-X). EDS spectrum images were acquired by serially scanning across a defined area of the specimen and recording cumulative EDS spectra at each position.

Samples were polished (to electron transparency) using an ion mill PIPS 691 (Gatan, USA).

The crystalline phases present in the ground samples were identified using X-ray diffraction (XRD) (Panalytical Empyrean, Netherlands, Cu Kα radiation).

2.3. Electrical resistivity

Samples were cut into 10 mm x 10 mm x 0.3 mm square-shaped pieces. Then small Indium balls for preparation of the contacts were placed into the sample corners and annealed at 300 °C for 3 min in N_2 atmosphere to remove the moisture from the samples. The *dc* measurement at ambient conditions were performed by standard four-point Van der Pauw method [22].

For the temperature dependent electrical conductivity, samples were placed into the holder and the resistor heater was used to perform the measurements under variable temperature (320 – 440 K) under vacuum (10 Pa). The *ac* conductivity was measured with 2 probe method. The data were obtained by collecting the impedance using the LCR-meter WK 6500B (WayneKerr, UK) at frequency of 1 kHz with the bias current of 100 mA. The upper contact on the sample was made up of the gold-plated tip, the bottom contact was formed by a chrome-plated copper plate. The leads from this contact are led to the BNC connectors and then to the LCR meter. Contacts of samples were created by Au-sputtering using Hummer II (Technics EMS, Inc., USA). Fig. 1 shows the schematic diagram of the measuring system.

2.4. Spreading resistance imaging (SRI)

The SRI was evaluated in the scanning system NTegra (NT-MDT Spectrum Instruments, Russia). SRI is an electrical characterization technique, based on scanning probe microscopy (SPM) to probe the two-dimensional resistivity distribution. Measurements were performed in contact mode with platinum coated conducting tip at constant force mode under nitrogen atmosphere to investigate the electrical response of the sample. Before the characterization, sample was ion beam etched using an ion mill PIPS 691 (Gatan, USA).

2.5. Magnetic measurements

Magnetic properties were measured using a MPMSXL7 SQUID magnetometer (Quantum Design, USA) operating in the 1.8 - 300 K range. Isothermal magnetization vs. field curves, *M(H)*, were measured up to 7 T field at two different temperatures 2 and 300 K. Magnetization vs. temperature curves were measured in two ways: at first, the sample was cooled down from room temperature (RT) to 5 K without applying any magnetic field (using ultra low field option to set zero field) and then heated back to RT under applied magnetic field of 5 mT (zero field cooled - ZFC curve); afterwards, under the same field the sample was cooled down again to 5 K and the magnetization was measured, following the same steps as before (field cooled - FC curve). The data were corrected to contribution of sample holder and normalized to weight of the samples.

3. Results and discussion

Table 4 shows the densities of sintered samples. Sample SiCN30 has 91.7 % of theoretical density. Samples with addition of 40 and 50 mass % of Ti-NbC phase were almost fully dense, with relative densities higher than 97 %. It is evident that the relative density of the composites is increasing with the addition of Ti-NbC.

3.1. Microstructure and XRD analysis

XRD analysis showed that the SiC is present in the composites in two modifications, as β-SiC and α-SiC which is a result of β-α transformation. Ti and NbC are present in the composites as a $(Ti, Nb)C_{ss}$. Amount of α-SiC in composites is increasing by increasing of $(Ti, Nb)C_{ss}$ content. Small amount of $NbSi_2$ phase was detected in all samples. We assume that Nb from NbC formed alloy with Si present as impurity in the starting powders (Tab. 1).

Microstructures of a polished and plasma etched surface of the SiCN composites are shown in the Fig. 4. The microstructures are composed from equiaxed and elongated SiC grains (dark grey) and from grains of $(TiNb)C_{ss}$ which are overetched. Between SiC grains there is grain boundary phase which is visible especially in SiCN50 composite. The presence of elongated SiC grains suggests its transformation from β to α. This is in agreement with XRD analysis. SiCN30 composite (Fig. 4a) contains some pores which corresponds to lower relative density of this sample. Some grains are pulled out from the surface of the SiCN40 and SiCN50 composites during grinding and polishing.

3.2. Transmission electron microscopy

TEM image and map of elements of the SiCN50 are shown in the Fig. 5. In the TEM image SiC grain and TiNbC grains are visible. On the grain boundary there are triple points with two different compositions. In the first type, Al, Ca, Si and O elements were detected. This indicates the formation of SiO_2-Al_2O_3-CaO glass during densification. The presence of these elements in the triple point is surprising because their content in the starting powder is a few hundreds of ppm (Tab. 1). However, high local concentration of these elements can be explained by its segregation during the densification process. Similar segregation of aluminum in the triple points of SiC or iron in the Si_3N_4 ceramics were observed earlier [21, 23].

On the other hand, there is a Fe, Co, Nb and Si rich region in the second type of triple points. Due to the absence of oxygen, we expected that $Fe_{1-x}Co_xSi$ alloys were formed based on ternary phase diagram (Fig. 6) [24].

From these results we assume that SiO_2-Al_2O_3-CaO and $Fe_{1-x}Co_xSi$ subsystems can form a liquid phase (above 1200 °C) and can help to densify the SiC-Ti-NbC system. Also, the

partial β- to α-SiC phase transformation of composites supports the formation of liquid phase.

3.3. Electrical conductivity

Fig. 6 shows the room temperature DC electrical conductivity of SiCN composites as a function of TiNbC content. For monolithic SiC ceramic material, the electrical conductivity is around 110 S/m at room temperature. This value may be explained by the presence of turbostratic carbon areas in the triple points and also by the presence of the graphene layer on the grain boundaries [21]. This graphene layer can increase the electrical conductivity of the composites as it was published earlier [25]. With the incorporation of the 30 and 40 wt. % TiNbC electrical conductivity was enhanced to 1.9 x 10^4 S/m and 6.9 x 10^4 S/m, respectively. The electrical conductivity of the SiC/TiNbC composite experienced a dramatic increase to around 2.4 x 10^5 S/m, when the mass fraction of TiNbC reached 50 %. The conduction behavior of SiC/TiNbC composites showed a typical percolation feature. Above the percolation threshold, a conductive network was formed and thus a significantly enhanced conductivity was obtained. Electrical conductivity achieved in this work is the highest value of the conductivity of SiC composites comparing to other published values.

If we compare our results with the values achieved by Frajkorova et al. [19] where the same composition of the composites was used, we can say that the freeze drying and two step sintering method resulted to the improvement of the electrical conductivity of the composites (in case of SiCN50 two order of magnitude higher value in our work).

Fig. 7 shows the temperature dependence of the electrical conductivity of the SiC composites compared to monolithic SiC. The conductivity of the samples slightly above

room temperature (320K) is one order of magnitude lower than the values measured at room temperature (Fig. 6). This difference in the values can be explained as a result of different method used for investigation of room temperature and temperature dependent conductivity. While at room temperature DC conductivity measurements method was used, temperature dependent conductivity was collected by AC conductivity measurement.

The SiC composites exhibited semiconductive behavior above room temperature, i. e. increasing conductivity with increasing temperature. The same behavior was found for the monolithic SiC. Despite the fact that pure TiC and NbC exhibit metal behavior conductivity, prepared composites exhibited semiconductive behavior (according to temperature dependent conductivity). This indicates that the electrical current is led through SiC grains. On the other hand, the addition of TiNbC significantly increased the electrical conductivity of composite, so the TiNbC phase must play the role in the conductivity of the composite.

3.4. Atomic force microscopy

Fig. 8 a-b show the atomic force microscopy (AFM) image and the current distribution image, respectively, for the electrically conductive SiC with addition of the 50 mass % of Ti-NbC. On the image of the topography (Fig. 8a) SiC grains and $(TiNb)C_{ss}$ grains correspond to the dark and bright areas, and in the current distribution image, the surfaces of the low and high electrically conductive materials correspond the dark and bright areas, respectively. For the applied voltage (V_{tip} = + 2.5 V) Fig. 8b shows two distinguishable phases - conductive with current around 20-30 nA and less conductive with current around 10 nA. As it can be observed, there is a good correlation between topography and

current. Comparing the current map with topography the more conductive phase is in topography visible as non-etched phase.

The fact of detecting current at TiNbC grains indicates that these grains are electrically connected and form part of a conducting network within the composite. Frajkorová et al. suggested on possibility of formation homogeneously distributed conductive amorphous phase based on Ti-Nb-C-(O-Si) on the SiC grain boundaries which forms continuous network with (Ti, Nb)C_{ss} resulting in enhancement of electrical conductivity [19]. AFM analysis confirmed the suggestions of Frajkorova et al. that the conductive network is formed from TiNbC grains. On the other hand, TEM analysis of our samples did not confirm their suggestion that on the grain boundary there is a Ti-Nb-C-O-Si conductive phase. From our results we can say that conductive phase on the grain boundary is composed from Ti-Nb-(C)-Fe(Co) elements which form alloys.

3.5. Magnetic properties

It was published, that NbC exhibits superconductivity behavior near 11 K [26-28], TiC could be superconductive near 4 K [29] , so it was interesting to find out how NbC can influence the behavior of SiC/Ti-NbC composite. On this behalf magnetic measurements were carried out on the reference sample of SiC with no additives and also on the SiC with Ti-NbC addition.

Fig. 9(a) shows Zero field cool/Field cool (ZFC/FC) magnetization vs. temperature dependence of the prepared samples. Sample SiC ref. exhibits bifurcation of ZFC and FC curve, split of the curves occurs possibly at temperatures higher than 300 K. This bifurcation, together with a wide maximum at the ZFC curve at 70 K, indicates the existence of frustrated system containing ferromagnetic (FM) and antiferromagnetic

(AFM) interactions. Inverse FC susceptibility $1/\chi$(T) was analyzed according to the Curie-Weiss law:

$$\chi - \chi_0 = C/(T - \theta),$$

where χ_0 is the temperature independent contribution, C is the Curie-Weiss constant, T is the temperature and θ is the Weiss temperature. This gives us the positive value of θ_{HT} = 112.2 K in high temperature region (HT; 100 – 240 K), implying FM ordering; for the low temperature region (LT; 5 – 100 K) a negative value θ_{LT} = -102.6 K was obtained, which means possible AFM interactions.

Temperature dependence of magnetization for SiCN30 is negative in the region 50 - 300 K, its $1/\chi_m$ plot is almost linear and gives the value θ = 2.14 K, which means that only weak ferromagnetic interaction is present. Plot for SiCN40 shows bifurcation at T = 45 K, obtained Weiss temperatures are θ_{HT} = 10.5 K (30 – 300 K) and θ_{LT} = -5.4 K (5 – 30 K), so competing FM/AFM interactions are also present. SiCN50 has clearly visible peak (blocking temperature) on the ZFC plot and bifurcation at 70 K, signalizing stronger FM/AFM interactions. Values of Weiss temperature for this sample are θ_{HT} = -13.9 K (100 – 300 K) and θ_{LT} = 5.5 K (5 – 100 K). Fig. 9(b) presents low-temperature M(T) behavior of the composites. All of them exhibit strong decrease of magnetization under 2K, where possibly superconducting state is reached.

Magnetization vs. Field (MH) loops measured at 2 K are presented in the Fig. 10(a). SiC ref. sample shows FM like behavior with visible hysteresis and saturation, with diamagnetic contribution at higher field. Samples SiCN30, SiCN40 and SiCN50 are paramagnetic, with no visible hysteresis, SiCN30 and SiCN40 show also diamagnetic contribution at higher field. MH loops measured at 300 K (fig. 10(b)) confirmed FM behaviour of SiC ref. sample, again there is visible diamagnetic slope at high field region.

Both SiCN30 and SiCN40 are diamagnetic, SiCN50 shows paramagnetic (PM) behaviour.

Very interesting is the observed superconductivity of SiCN30 and SiCN40. Type-I superconductivity was reported earlier in B-doped 3C-SiC and 6H-SiC under $T_C \sim 1.4$ K (critical temperature) [30], as well as type-II superconductivity in Al-doped 3C-SiC [31].

To confirm our results observed in the ZFC/FC measurements, low-field MH loops were measured at 2 K (fig. 11). SiCN30 shows (fig. 11(a)) the superconductivity, where initial low-field magnetization firstly decreases with field almost linearly and then increases because of superposition of FM component. With increasing of the amount of Ti-NbC phase the superconductive state starts to disappear (SiCN40; Fig. 11(b)) and SiCN50 shows at given temperature weak ferromagnetism (fig. 11(c)). We assume that together with the addition of Ti and NbC we incorporate the impurities from the initial powders, especially Fe and Co, which suppress the superconductivity.

It was reported that α-SiC is diamagnetic [32] but defect-induced FM may occur when the SiC is exposed to Xe ion radiation. Also β-SiC was reported as ferromagnetic [33]. On the other hand, doping with Al [34] or vanadium carbide [33] could reduce the FM in the SiC. In case of this study, FM in SiC ref. is similar to (Al, Fe) codoped SiC reported earlier [35] and is mainly caused by Fe impurities in the starting powder. Visible diamagnetic slope, both on the 2 K and 300 K MH curves (Fig. 10) indicates that SiC matrix itself is diamagnetic. However, samples with addition of Ti and NbC were prepared from different starting SiC powder (different batch) comparing to SiC ref. and thus obtained recognizable different level of Fe contamination.

4. Conclusions

Silicon carbide composites with 30, 40 and 50 wt. % of of Ti and NbC as sintering additives were prepared by hot-press method. The combination of the planetary ball milling and spraying the suspension into the liquid nitrogen led to homogeneous distribution of conductive phase in the starting powder. The use of the two step sintering process avoided to squeezing out of the melted Ti, which led to prepare of the dense SiC composites with addition of 40 and 50 wt. % of Ti-NbC. Highest electrical conductivity 2.4 x 10^5 S/m was achieved in the composite with addition of 50 wt. % of Ti-NbC by homogeneous distribution of Ti and NbC in SiC matrix and formation of the conductive network from TiNbC grains. Prepared composites show complex magnetic properties, diamagnetism originated from SiC matrix, paramagnetism caused by Ti and NbC admixing, as well as weak ferromagnetism probably coming from impurities contained in the initial powders. Samples with 30 and 40 wt % of Ti and NbC exhibit superconducting state below 2 K. The origin of superconductivity is not yet clear and we will try to explain it in our further work.

Declaration of competing interest

The authors declare that they have no known competing financial interests or personal relationships that could have appeared to influence the work reported in this paper.

Acknowledgements

This study was performed during the implementation of the project Building-up Centre for advanced materials application of the Slovak Academy of Sciences, ITMS project code 313021T081 supported by Research & Innovation Operational Programme funded by the ERDF. This work was partially supported from the European Union's Horizon 2020 research and innovation programme under grant agreement No. 810701. The support of VEGA 2/0007/21 and APVV-19-410 projects is also acknowledged.

Authors would like to thank Dr. Peter Švec Jr. (Institute of Physics, Slovak Academy of Sciences) for the TEM analysis.

References

[1] C. Martin, B. Cales, P. Vivier, P. Mathieu, Electrical discharge machinable ceramic composites, Mater. Sci. Eng. A109 (1989) 351–356. https://doi.org/10.1016/0921-5093(89)90614-X.

[2] O. Malek, J. González-Julián, J. Vleugels, W. Vanderauwer, B. Lauwers, M. Belmonte, Carbon nanofillers for machining insulating ceramics, MaterToday 14 (2011) 496–501. https://doi.org/10.1016/S1369-7021(11)70214-0.

[3] B. Lauwers, J.P.Kruth, W. Liu, W. Eeraerts, B. Schacht, P. Bleys, Investigation of material removal mechanisms in EDM of composite ceramic materials, J. Mater. Process. Technol. 149 (2004) 347–352. https://doi.org/10.1016/j.jmatprotec.2004.02.013.

[4] G. Sauti, A. Can, D.S. McLahlan, The AC conductivity of liquid-phase-sintered silicon carbide, J. Am. Ceram. Soc. 90 (2007) 2446–2453. https://doi.org/10.1111/j.1551-2916.2007.01792.x.

[5] K.J. Kim, K.Y. Lim, Y.W. Kim, M.J. Lee, W.S. Seo, Electrical resistivity of α-SiC ceramics sintered with Al_2O_3 or AlN additives, J. Eur. Ceram. Soc. 34 (2014) 1695–1701. https://doi.org/10.1016/j.jeurceramsoc.2014.01.004.

[6] G.D. Zhan, M. Mitomo, A.K. Mukherjee, Effects of heat treatment and sintering additives on thermal conductivity and electrical resistivity in fine-grained SiC ceramics, J. Mater. Res. 17 (2002) 2327–2333. https://doi.org/10.1557/JMR.2002.0341.

[7] A. Can, D.S. McLachlan, G. Sauti, M. Herrmann, Relationships between microstructure and electrical properties of liquid-phase sintered silicon carbide materials using impedance spectroscopy, J. Eur. Ceram. Soc. 27 (2007) 1361–1363. https://doi.org/10.1016/j.jeurceramsoc.2006.05.053.

[8] F. Siegelin, H.J. Kleebe, L.S. Sigl, Interface characteristics affecting electrical properties of Y-doped SiC, J. Mater. Res. 18 (2003) 2608–2617. https://doi.org/10.1557/JMR.2003.0365.

[9] Y.W. Kim, S. Kultayeva, J. Sedláček, O. Hanzel, P. Tatarko, Z. Lenčéš, P. Šajgalík, Thermal and electrical properties of additive-free rapidly hot-pressed SiC ceramics, J. Eur. Ceram. Soc. 40 (2020) 234–240. https://doi.org/10.1016/j.jeurceramsoc.2019.10.015.

[10] Y.W. Kim, K. J. Kim, H.C. Kim, N.H. Cho, K.Y. Lim, Electrodischarge-machinable silicon carbide ceramics sintered with yttrium nitrate, J. Am. Ceram. Soc. 94 (2011) 991–993. https://doi.org/10.1111/j.1551-2916.2011.04419.x.

[11] M. Michálek, J. Sedláček, M. Parchoviansky, M. Michálková, D. Galusek, Mechanical properties and electrical conductivity of alumina/MWCNT and alumina/zirconia/MWCNT composites, Ceram. Int. 40 (2014) 1289-1295. https://doi.org/10.1016/j.ceramint.2013.07.008.

[12] O. Hanzel, J. Sedláček, P. Šajgalík, New approach for distribution of carbon nanotubes in alumina matrix, J. Eur. Ceram. Soc. 34 (2014) 1845–1851. https://doi.org/10.1016/j.jeurceramsoc.2014.01.020.

[13] A. Kovalčíková, Cs. Balázsi, J. Dusza, O. Tapasztó, Mechanical properties and electrical conductivity in a carbon nanotube reinforced silicon nitride composite, Ceram. Int. 38 (2012) 527–533. https://doi.org/10.1016/j.ceramint.2011.07.038.

[14] Cs. Balázsi, B. Fényi, N. Hegman, Zs. Kövér, F. Wéber, Z. Vértesy, Z. Kónya, I. Kiricsi, L.P. Biró, P. Arató, Development of CNT/Si_3N_4 composites with improved mechanical and electrical properties, Composites: Part B 37 (2006) 418–424. https://doi.org/10.1016/j.compositesb.2006.02.006.

[15] K. Lee, Ch.B. Mo, S.B. Park, S.H. Hong, Mechanical and electrical properties of multiwalled CNT-Alumina nanocomposites prepared by a sequential two-step processing of ultrasonic spray pyrolysis and spark plasma sintering, J. Am. Ceram. Soc. 94 (2011) 3774–3779. https://doi.org/10.1111/j.1551-2916.2011.04689.x.

[16] G. Yamamoto, M. Omori, T. Hashida H. Kimura, A novel structure for carbon nanotube reinforced alumina composites with improved mechanical properties, Nanotech. 19 (2008) 315708-315713. https://doi.org/10.1088/0957-4484/19/31/315708.

[17] B. Román-Manso, E. Domingues, F.M. Figueiredo, M. Belmonde, P. Miranzo, Enhanced electrical conductivity of silicon carbide ceramics by addition of graphene nanoplatelets, J. Eur. Ceram. Soc. 35 (2015) 2723-2731. https://doi.org/10.1016/j.jeurceramsoc.2015.03.044.

[18] S.J. Schneider Jr., Engineered Materials Handbook, Vol. 4, Ceramics and Glasses, ASM International, USA, 1991.

[19] F. Frajkorová, Z. Lenčéš, P. Šajgalík, Electrically conductive silicon carbide without oxide sintering additives, J. Kor. Ceram. Soc. 49 (2012) 342-346. https://doi.org/10.4191/kcers.2012.49.4.342.

[20] M. Balog, P. Šajgalík, F. Hofer, P. Warbichler, K. Frohlich, O. Vávra, J. Janega, J.L. Huange, Electrically conductive SiC–$(Nb,Ti)_{ss}$–$(Nb,Ti)C_{ss}$ cermet, J. Eur. Ceram. Soc. 26 (2006) 1259–1266. https://doi.org/10.1016/j.jeurceramsoc.2005.01.038

[21] P. Šajgalík, J. Sedláček, Z. Lenčéš, J. Dusza, H.T. Lin, Additive-free hot-pressed silicon carbide ceramics-A material with exceptional mechanical properties, J. Eur. Ceram. Soc. 36 (2016) 1333-1341. https://doi.org/10.1016/j.jeurceramsoc.2015.12.013.

[22] L.J. van der Pauw, A method of measuring specific resistivity and hall effect of discs of arbitrary shape, Philips Res. Repts 13(1958) 1-9.

[23] K. Rajan, P. Šajgalík, Local chemistry changes in Si_3N_4 based ceramics during hot-pressing and subsequent annealing, J. Eur. Ceram. Soc. 19 (1999) 2027–2032. https://doi.org/10.1016/S0955-2219(99)00014-X.

[24] L. Rokhlin, Cobalt-Iron-Silicon, in: G. Effenberg, S. Ilyenko, Ternary Alloy Systems, Springer Berlin Heidelberg, New York, 2008, pp. 1-26.

[25] J.H. Eom, Y.W. Kim, K.J. Kim, W.S. Seo, Improved electrical and thermal conductivities of polysiloxane-derived silicon oxycarbide ceramics by barium addition, J. Eur. Ceram. Soc. 38 (2018) 487–493. https://doi.org/10.1016/j.jeurceramsoc.2017.09.045.

[26] M. Wells, M. Pickus, K. Kennedy, V. Zackay, Superconductivity of solid solutions of TaC and NbC, Phys. Rev. Lett. 12 (1964) 536-538. https://doi.org/10.1103/PhysRevLett.12.536.

[27] H.X. Geng, G.C. Che, W.W. Huang, S.L. Jia, H. Chen, Z.X. Zhao, Structural, morphological, C content and T_C changes of the NbC superconductor prepared by Nb powder and carbon nanotubes, Supercond. Sci. Technol. 20 (2007) 211–215. https://doi.org/10.1088/0953-2048/20/3/016.

[28] R. Jha, V.P.S. Awana, Vacuum encapsulated synthesis of 11.5 K NbC superconductor, J. Supercond. Nov. Magn. 25 (2012) 1421–1425. https://doi.org/10.1007/s10948-012-1654-6.

[29] N. Guskos, V. Likodimos, S. Glenis, G. Zolnierkiewicz, J. Typek, C.L. Lin, A. Biedunkiewicz, Magnetic properties of TiC_x/C nanocomposites, J. Non Cryst. Solids 354 (2008) 4330-4333. https://doi.org/10.1016/j.jnoncrysol.2008.06.046.

[30] Z. A. Ren, J. Kato, T. Muranaka, J. Akimitsu, M. Kriener, Y. Maeno, 2007. Superconductivity in boron-doped SiC, J. Phys. Soc. Jpn. 76, 103710. https://doi.org/10.1143/JPSJ.76.103710.

[31] T. Muranaka, Y. Kikuchi, T. Yoshizawa, N. Shirakawa, J. Akimitsu, 2008. Superconductivity in carrier-doped silicon carbide, Sci. Technol. Adv. Mater. 9, 044204. https://doi.org/10.1088/1468-6996/9/4/044204

[32] Y. Wang, Y. Liu, G. Wang, W. Anwand, C.A. Jenkins, E. Arenholz, F. Munnik, O.D. Gordan, G. Salvan, D.R.T. Zahn, X. Chen, S. Gemming, M. Helm, S. Zhou, 2015. Carbon *p* electron ferromagnetism in silicon carbide. Sci. Rep. 5, 8999. https://doi.org/10.1038/srep08999.

[33] H. Wang, Ch. Yan, H. Kong, J. Chen, J. Xin, E. Shi, Influence of mole ratio of Si:C on the magnetic property of undoped and vanadium carbide doped 3C-SiC, Chem. Phys. Lett. 556 (2013) 142-145. https://doi.org/10.1016/j.cplett.2012.12.008.

[34] C. Zhang, J. Lian, H.L.Ng. Dickon, Magnetic properties of Al-doped B_4C and SiC ceramics, J. Amer. Ceram. Soc. 96 (2013) 3494-3499. https://doi.org/10.1111/jace.12510.

[35] B. Song, X.L. Chen, J.C. Han, J.K. Jian, H.Q. Bao, H. Li, K.X. Zhu, W.Y. Wang, G. Wang, H.B. Zuo, (2010). Structural and magnetic properties of (Al, Fe)-codoped SiC, J. Phys. D: Appl. Phys. 43, 415002. https://doi.org/10.1088/0022-3727/43/41/415002.

Tables

Tab. 1 Impurities in the initial powders

Element	**SiC**	**NbC**	**Ti**
	ppm	**ppm**	**ppm**
Ca	594	227	245
Fe	2150	1190	1260
Co	–	535	–
Al	3130	448	428
Si	99	113	482

Tab. 2 Chemical composition of starting mixtures

	W [wt. %]		
Sample	**SiC**	**Ti**	**NbC**
SiC30TiNbC	70	10.8	19.2
SiC40TiNbC	60	14.4	25.6
SiC50TiNbC	50	18.0	32.0

Tab. 3 Density of initial powders

Powder	**SiC**	**Ti**	**NbC**
ρ **[g/cm^3]**	3.21	4.51	7.8

Tab. 4 The density and relative density of reference SiC [21] and composites after sintering at 1850 °C

Sample	**ρ [g/cm^3]**	**TD [%]**
SiC ref.	3.21	99.9
SiCN30	3.44	91.7
SiCN40	3.86	97.2
SiCN50	4.14	98.3

Figures

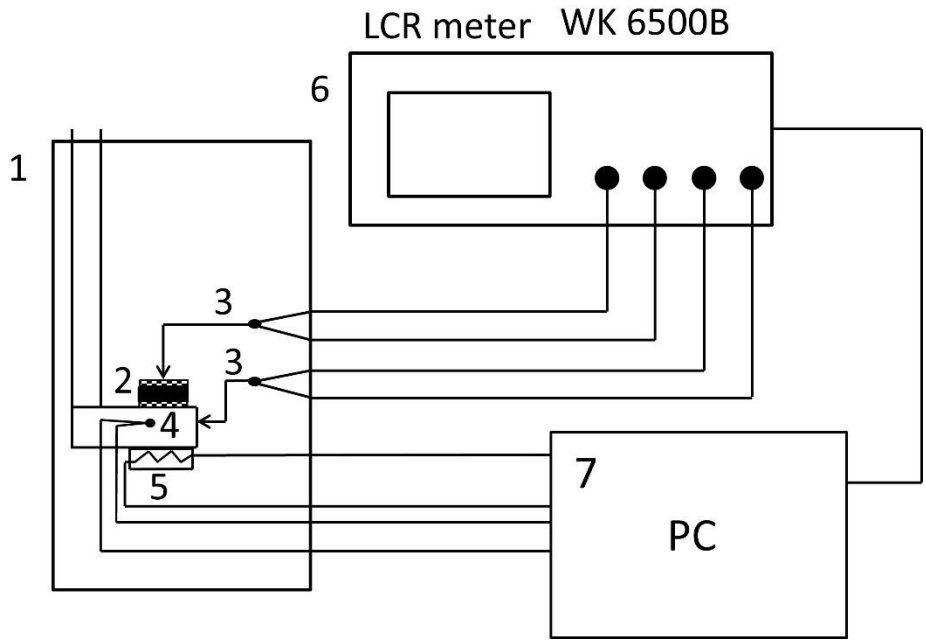

Fig. 1 Schematic diagram of temperature dependent conductivity measurement. The heated holder is (1), which is composed from the sample holder (2), probes (3), thermocouple (4) and the resistor heater (5). LCR meter is (6), PC is personal computer (7).

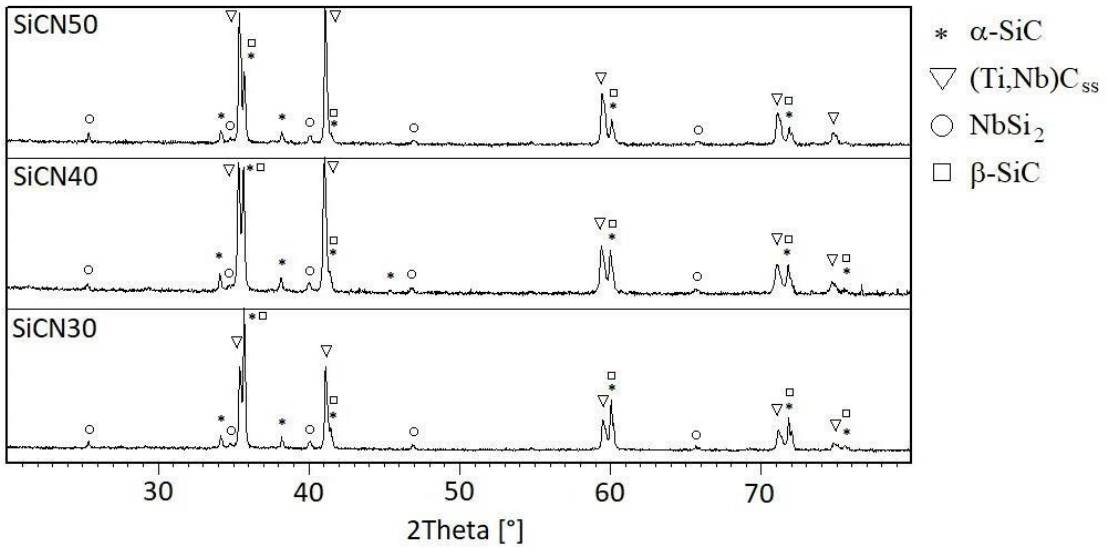

Fig. 2 Comparison of XRD patterns of sintered samples

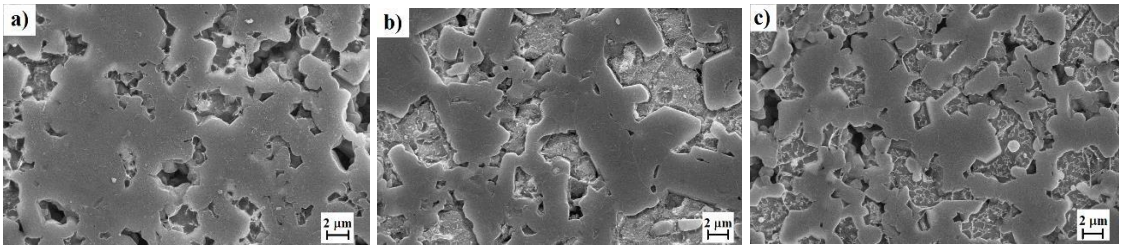

Fig. 4 The microstructures of sintered samples SiCN30 (a), SiCN40 (b), SiCN50 (c), dark grey represents SiC grains, (Ti, Nb)C_{ss} grains are overetched

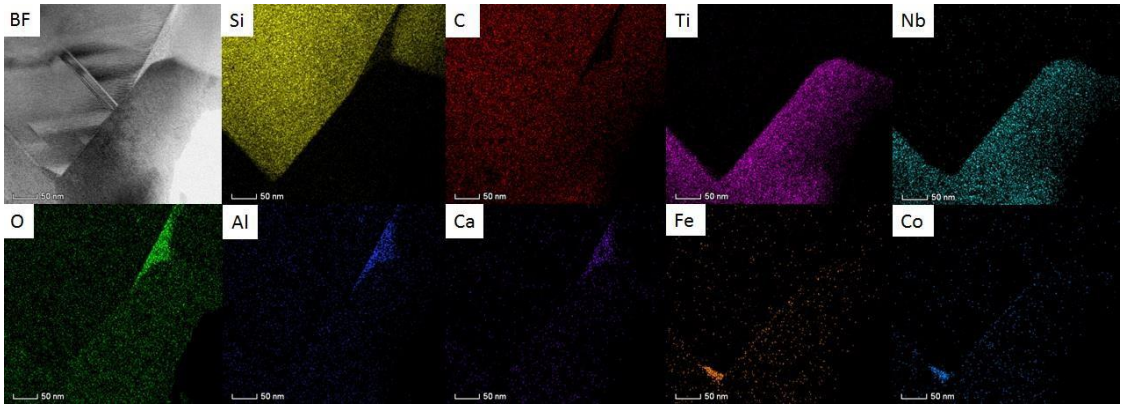

Fig. 5 TEM image and EDX map image of the sample SiCN50

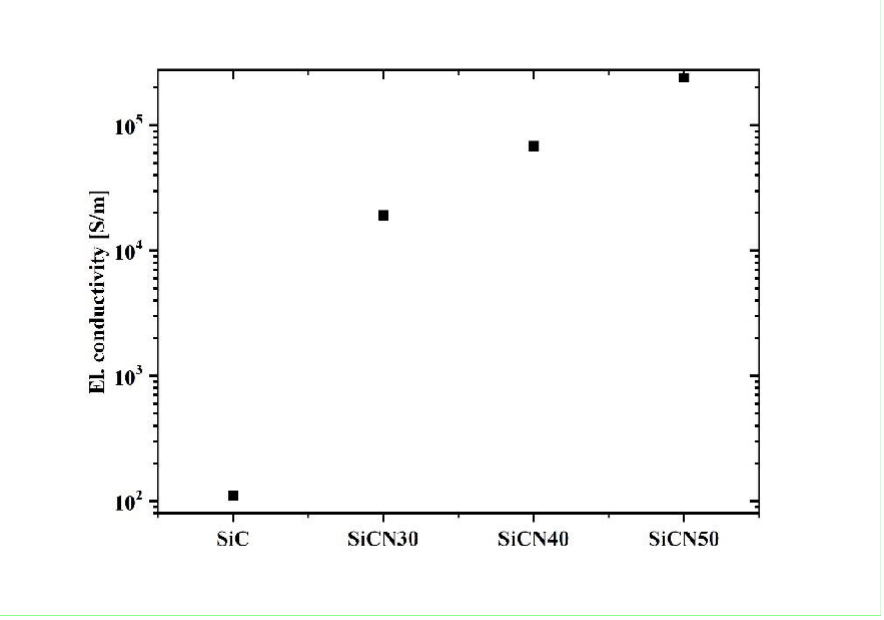

Fig. 6 Room temperature electrical conductivity of composites as a function of TiNbC content

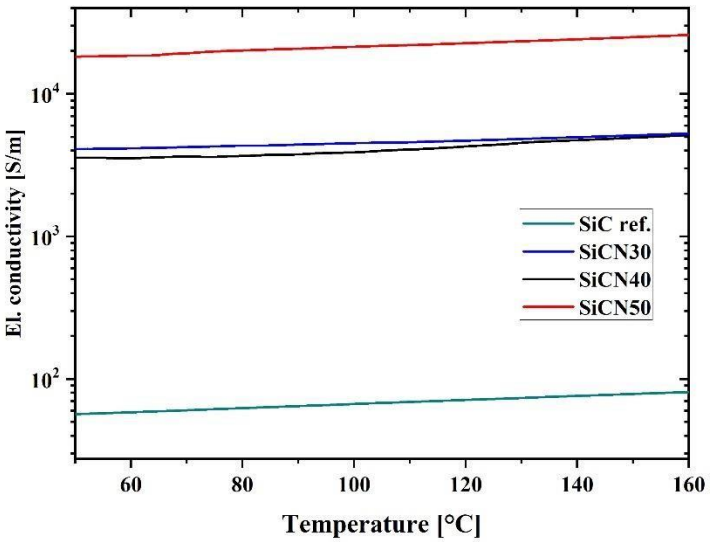

Fig. 7 Temperature dependence of the electrical conductivity of the various samples

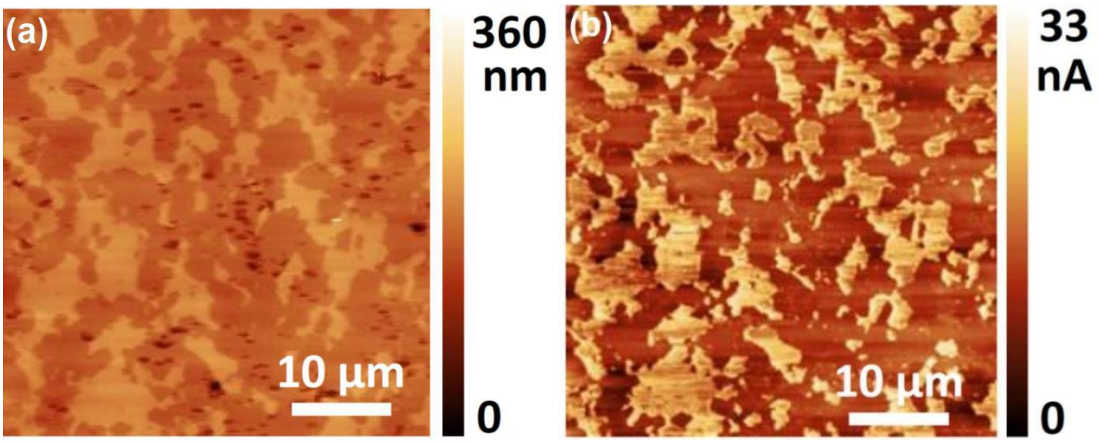

Fig. 8 Topography of SiCN50 (a) and current map of the same surface area acquired at Vtip = + 2.5 V (b)

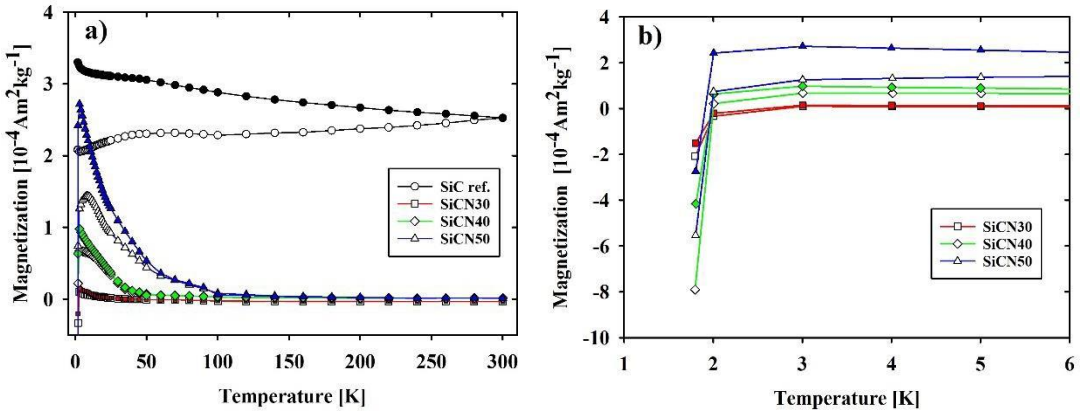

Fig. 9 ZFC (empty symbols) and FC (full symbols) curves for SiC ref. (circle), SiCN30 (square), SiCN40 (diamond), SiCN50 (triangle) (a), enlarged view of the low-temperature part of the ZFC and FC curves (b).

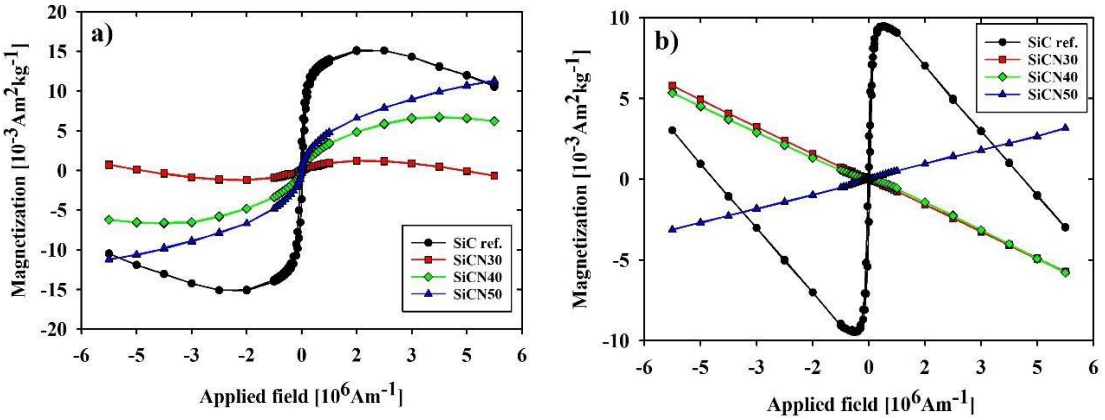

Fig. 10 MH loops measured at 2 K (a) and 300 K (b) for SiC_{ref} (circle), SiCN30 (square), SiCN40 (diamond), SiCN50 (triangle).

Fig. 11 Low-field MH loops measured at 2 K for SiCN30 (a), SiCN40 (b) and SiCN50.